Society For Biomaterials

Effect of ceramic calcium–phosphorus ratio on chondrocyte-mediated biosynthesis and mineralization

Margaret K. Boushell,[1] Nora T. Khanarian,[1] Raquel Z. LeGeros,[2] Helen H. Lu[1]

[1]Biomaterials and Interface Tissue Engineering Laboratory, Department of Biomedical Engineering, Columbia University, New York 10027

[2]Calcium Phosphate Research Laboratory, Department of Biomaterials and Biomimetics, New York University College of Dentistry, New York 10010

Received 5 February 2017; revised 3 April 2017; accepted 19 May 2017
Published online 21 June 2017 in Wiley Online Library (wileyonlinelibrary.com). DOI: 10.1002/jbm.a.36122

Abstract: The osteochondral interface functions as a structural barrier between cartilage and bone, maintaining tissue integrity postinjury and during homeostasis. Regeneration of this calcified cartilage region is thus essential for integrative cartilage healing, and hydrogel-ceramic composite scaffolds have been explored for calcified cartilage formation. The objective of this study is to test the hypothesis that Ca/P ratio of the ceramic phase of the composite scaffold regulates chondrocyte biosynthesis and mineralization potential. Specifically, the response of deep zone chondrocytes to two bioactive ceramics with different calcium–phosphorus ratios (1.35 ± 0.01 and 1.41 ± 0.02) was evaluated in agarose hydrogel scaffolds over two weeks *in vitro*. It was observed that the ceramic with higher calcium–phosphorus ratio enhanced chondrocyte proliferation, glycosaminoglycan production, and induced an early onset of alkaline phosphorus activity, while the ceramic with lower calcium–phosphorus ratio performed similarly to the ceramic-free control. These results underscore the importance of ceramic bioactivity in directing chondrocyte response, and demonstrate that Ca/P ratio is a key parameter to be considered in osteochondral scaffold design. © 2017 Wiley Periodicals, Inc. J Biomed Mater Res Part A: 105A: 2694–2702, 2017.

Key Words: chondrocyte, hydrogel, calcium-deficient apatite, calcified cartilage, interface

How to cite this article: Boushell MK, Khanarian NT, LeGeros RZ, Lu HH. 2017. Effect of ceramic calcium–phosphorus ratio on chondrocyte-mediated biosynthesis and mineralization. J Biomed Mater Res Part A 2017:105A:2694–2702.

INTRODUCTION

Osteoarthritis is characterized by articular cartilage degeneration which causes severe pain and leads to loss of joint motion. This debilitating condition currently affects over 27 million Americans,[1] with an estimated societal cost of approximately $100 billion.[2] Since cartilage has a limited capacity for self-repair,[3] surgical intervention such as microfracture, mosaicplasty, or autologous chondrocyte implantation is required to treat this condition. The long-term clinical success of these techniques is hindered by donor-site morbidity, poor graft integration, and the formation of fibrocartilaginous tissue, which is nonphysiologic and mechanically inferior to hyaline cartilage.[4–7]

To overcome these limitations, tissue engineered osteochondral grafts have been investigated as promising alternatives for cartilage repair.[8–18] One of the challenges in this approach is maintaining a stable barrier between the cartilage and bone during the healing process. The presence of a physical barrier has been shown to prevent unwanted vascular invasion from subchondral bone during cartilage healing,[19] and it is also needed to ensure long-term cartilage integrity and homeostasis. The native osteochondral interface consists of a mineralized cartilage matrix containing collagen II, proteoglycans, and calcium phosphate.[20,21] Its functions include anchoring articular cartilage to the subchondral bone and enabling effective force transfer from cartilage to bone.[22,23] The calcified cartilage layer is critical to maintain cartilage integrity because it acts as a physical barrier that prevents vascular invasion from the underlying bone. The physical barrier is reported to be essential during full-thickness lesion healing because, in the absence of a structural barrier, the cartilage is compromised by osseous upgrowth.[19] Regeneration of this calcified interface is therefore essential for integrative and stable cartilage repair.

Current osteochondral interface tissue engineering efforts began with cell-based approaches,[24] followed by more recent reports of scaffold-based approaches, such as an agarose-hydroxyapatite (HA) composite scaffold for calcified cartilage

Correspondence to: H.H. Lu; Department of Biomedical Engineering, Columbia University, 351 Engineering Terrace Building, MC 8904, 1210 Amsterdam Avenue, New York, NY 10027; e-mail: hhlu@columbia.edu
Contract grant sponsor: the National Institutes of Health; contract grant number: R01-AR055280, HHL
Contract grant sponsor: The Presidential Early Career Award for Scientists and Engineers (PECASE, HHL)
Contract grant sponsor: The National Institutes of Health Ruth L. Kirschstein National Research Service Award; contract grant number: T32 AR059038 (MKB/NTK)
Contract grant sponsor: The CTICE Fellowship (MKB), and the National Science Foundation (Graduate Research Fellowship, NTK)

formation.[25,26] Agarose exhibits a fast gelation time, allowing for homogenous distribution of mineral and cells within the constructs. Furthermore, higher mechanical properties were measured for deep zone chondrocyte-seeded agarose hydrogels than those of other hydrogels, such as alginate.[26] However, triiodothyronine (T3), in combination with HA, was necessary to promote matrix elaboration by chondrocytes in agarose-HA constructs.[26] While T3 is naturally occurring, hormone stimulation is an additional step that increases cost and complexity of care which is not ideal for clinical translation. As an alternative to T3, it is hypothesized here that the calcium phosphate composition can be optimized to promote matrix elaboration in a hormone-free environment. While the effect of calcium–phosphorus ratio on chondrocyte response has not been extensively investigated, published studies have reported that changes in the calcium–phosphorus ratio of ceramics can modulate the adhesion, proliferation, and matrix deposition of a variety of cells including osteoblasts, fibroblasts, and mesenchymal stem cells.[27–30]

Inspired by these findings, the objective of this study is to test the hypothesis that changes in ceramic composition, as reflected in its calcium–phosphorus ratio, will regulate deep zone chondrocyte response in a hydrogel-ceramic composite scaffold. Since the mineral of the native calcified cartilage has been reported to be a poorly crystalline, carbonated hydroxyapatite,[20] this study will form the interface scaffolds using two poorly crystalline hydroxyapatite particles with differing calcium–phosphorus ratios. The response of deep zone chondrocytes will be tested, as their ability to form mineralized cartilage has been demonstrated previously.[24,31] It is hypothesized that the calcium–phosphorus ratio of bioactive ceramics ($Ca/P < 1.67$) can be tuned to increase the amount of glycosaminoglycan (GAG)- and collagen-rich matrix produced by this interface-relevant cell population within agarose scaffolds, independent of T3 stimulation. The findings of this study will provide new insights regarding cell–ceramic interactions and guide scaffold design for osteochondral interface tissue engineering.

MATERIALS AND METHODS

Cells and cell culture

Primary deep zone chondrocytes were isolated and pooled from the femoral articular cartilage of five immature calf knees (Green Village Packing, Green Village, NJ) following published protocols.[32] Briefly, the deep zone, defined as the bottom third of the cartilage, was separated and the calcified cartilage was removed with a scalpel. The cartilage was then minced and digested with collagenase type 2 (310 u/mg, Worthington, Lakewood, NJ) for 16 hours in Dulbecco's Modified Eagle's Medium (DMEM) supplemented with 10% fetal bovine serum (FBS, Atlanta Biologicals, Atlanta, GA), 2% antibiotics (10,000 U/mL penicillin, 10 mg/mL streptomycin), and 0.2% antifungal (amphotericin B). The deep zone chondrocyte suspension was filtered before plating to remove digested extracellular matrix (30 μm, Spectrum, Rancho Dominguez, CA). The isolated cells were maintained in high-density culture in fully supplemented DMEM with 10% FBS, 1% nonessential amino acids, 1% penicillin-streptomycin, 0.1% gentamicin sulfate, and 0.1% antifungal for 72 hours prior to seeding in the hydrogel.[25] All media supplements were purchased from Cellgro-Mediatech unless otherwise specified.

Ceramic characterization

Calcium-deficient apatite (CDA) ceramic particles were purchased from Sigma-Aldrich (St. Louis, MO) and their calcium and phosphorus content ($n = 6$), crystal structure ($n = 2$), and chemical composition ($n = 2$) were determined. Particle morphology ($n = 2$) and size ($n = 20$) was assessed using brightfield microscopy (20x, Zeiss, Axiovert 25, Oberkochen, Germany) and scanning electron microscopy (SEM, 1000x, Hitachi S-4700, Pleasanton, CA). For SEM, particles were sputter-coated with gold for 20 seconds (Cressington 108 Auto, Watford, UK) and imaged at 5 kV. Ceramic calcium and phosphorus content ($n = 6$) was determined using inductively coupled plasma analysis (ICP, Thermo Jarrell Ash, Trace Scan Advantage, Franklin, MA).[33] Briefly, 10 mg of ceramic was dissolved in several drops of 17% HCl and brought to 100 mL with double distilled water. The resulting solution was pumped through argon plasma excited by a radiofrequency generator (2 kW/27.12 MHz). The concentration of the element of interest was determined using its characteristic wavelength (Ca, 317.9 Å; P, 213.6 Å).[33] The crystal structure of the ceramics was evaluated with X-ray diffraction (XRD, X-ray Diffractometer, Inel, Artenay, France), whereby the samples were scanned over a range of 0–120°, with a step size of 0.029°. Ceramic chemistry was further examined using Fourier transform infrared spectroscopy (FTIR, FTS 3000MX Excalibur Series, Digilab, Randolph, MA), wherein dehydrated samples were mixed with potassium bromide and scanned in absorbance mode (400 scans, 4 cm^{-1} resolution). Peaks of interest included phosphorus bending peaks (961, 1030–1080, 566–628 cm^{-1}), as well as hydroxyl (3568 cm^{-1}) and carbonate peaks (1415–1647, 870 cm^{-1}).

Scaffold fabrication, characterization, and culture

Deep zone chondrocytes were encapsulated at a density of 10 million cells/mL in 2% low-gelling agarose (Agarose Type VII, Sigma), and a biopsy punch (Sklar Instruments, West Chester, PA) was used to core cylindrical scaffolds ($Ø = 5$ mm, height = 2.4 mm).[26] Acellular and cellular agarose scaffolds with 1.5 w/v% ceramic (Sigma), added at the time of gelation, and corresponding controls without ceramic were fabricated. For cellular-ceramic scaffolds, the ceramic was added to the cell suspension before mixing with concentrated agarose.

Gross morphology of acellular scaffolds was assessed with a stereoscope (Olympus SZ61, Center Valley, PA) in both top and cross-sectional views. Ceramic distribution ($n = 2$) was visualized by environmental scanning electron microscopy (ESEM, 15 kV, JEOL 5600LV, Tokyo, Japan). Scaffold water content (wet weight-dry weight/wet weight, $n = 3$) was calculated following desiccation for 24 hours (CentriVap Concentrator, Labconco, Kansas City, MO). Elemental composition ($n = 2$) of the scaffolds was ascertained by energy dispersive X-ray analysis (EDAX, 15 kV, FEI Quanta 600, FEI, Hillsboro, OR). The

crystallinity of the hydrogel-ceramic composites was confirmed by X-ray diffraction of the dehydrated scaffolds. Scaffold mechanical properties ($n = 3$) were determined on a shear-strain controlled rheometer (TA instruments, New Castle, DE) following published protocols.[26] Briefly, each sample was placed between two flat porous platens and immersed in PBS to prevent dehydration. First, the equilibrium compressive Young's modulus (Eeq) was calculated at 15% compressive strain. Secondly, a dynamic shear test was performed (0.01–10 Hz) with a logarithmic frequency sweep at a shear strain amplitude of 0.01 radian. Both the magnitude of the complex shear modulus and phase shift angle between the applied strain and the resulting torque were determined at 1 Hz.

To assess cell response, all samples were cultured under humidified conditions at 37°C and 5% CO_2, and maintained in ITS medium composed of DMEM supplemented with 1% ITS+ Premix (BD Biosciences, San Jose, CA), 1% penicillin-streptomycin, 0.1% gentamicin sulfate, 0.1% antifungal, and 40 μg/mL L-proline (Sigma). The medium was changed every other day and freshly supplemented with 50 μg/mL ascorbic acid (Sigma). The responses of deep zone chondrocytes in CDA-1, CDA-2, and ceramic-free scaffolds were compared over a two-week culture period. Specifically, cell viability, growth, collagen and glycosaminoglycan (GAG) deposition, mineralization, and hypertrophy were compared between groups as well as over time.

Cell proliferation and viability

Cell viability ($n = 2$) was visualized using Live/Dead staining (Molecular Probes, Eugene, OR), following the manufacturer's suggested protocol. After rinsing with phosphate buffered saline (PBS), samples were imaged at excitation and emission wavelengths of 488 and 568 nm, respectively (Zeiss, Axiovert 25). Cell proliferation ($n = 5$) was determined using the Quanti-iT™ PicoGreen® dsDNA assay kit (Molecular Probes, Eugene, OR) following sample digestion. Briefly, the sample was rinsed with PBS and exposed to a freeze–thaw cycle in 500 μL of 0.1% Triton-X solution (Sigma) in order to lyse the cells. After desiccation for 12 hours in a CentriVap Concentrator (Labconco), the samples were digested for 18 hours at 65°C with papain (8.3 activity units/mL) in 0.5 mL of digestion buffer (0.1*M* sodium acetate (Sigma), 10 m*M* cysteine HCl (Sigma), and 50 m*M* ethylenediaminetetraacetate (Sigma)). For DNA content, a 25 μL aliquot of the sample was mixed with 175 μL of the PicoGreen® working solution and fluorescence was measured with a microplate reader (Tecan, Research Triangle Park, NC), at excitation and emission wavelengths of 485 and 535 nm, respectively. The conversion factor of 7.7 pg DNA/cell was used to determine cell number.[34]

Matrix deposition

Total collagen content ($n = 5$) was quantified using a modified hydroxyproline assay[35] with bovine collagen I solution (Biocolor, Carrickfergus, UK) as the standard. Briefly, a 40 μL aliquot of sample digest was mixed with 10 μL of 10*N* sodium hydroxide and heated to 250°C for 25 min in order to hydrolyze the collagen. The hydrolyzate was then oxidized at room temperature for 25 min with 450 μL of buffered Chloramine T reagent, prior to the addition of Ehrlich's reagent (15% *p*-dimethylaminobenzaldehyde in 2:1 isopropanol/percholoric acid). Absorbance was measured at 555 nm with a microplate reader (Tecan). All matrix values were normalized by sample wet weight in order to account for any differences in sample size. Additionally, collagen distribution ($n = 2$) was evaluated via histology. Briefly, the samples were first fixed in neutral buffered formalin with 1% cetylpyridinium chloride (Sigma) for 24 hours, followed by dehydration with an ethanol series. The dehydrated samples were embedded in paraffin (Paraplast X-tra Tissue Embedding Medium, Fisher Scientific, Waltham, MA) and 7 μm sections were obtained from the center of the scaffold. Paraffin was cleared with xylenes, the samples were rehydrated, stained with picrosirius red solution for 1 hour, and exposed to 0.1*N* hydrochloric acid for 2 min ($n = 2$). In addition, collagens I and II deposition were assessed using immunohistochemistry ($n = 2$).[26] Specifically, monoclonal antibodies for collagen I (1:100 dilution) and collagen II (1:100 dilution) were purchased from Abcam (Cambridge, MA). After fixation, samples were treated with 1% hyaluronidase for 30 min at 37°C and incubated with primary antibody overnight. Cell nuclei were stained with 4',6-diamidino-2-phenylindole (Sigma). A FITC-conjugated secondary antibody (1:200 dilution, LSAB2 Abcam) was used and samples were imaged under confocal microscopy (Olympus Fluoview IX70, Center Valley, PA) at excitation and emission wavelengths of 488 and 568 nm, respectively.

Sample GAG content ($n = 5$) was determined with a modified 1,9-dimethylmethylene blue (DMB) binding assay,[36–38] with chondrotin-6-sulfate (Sigma) as the standard. The absorbance difference between 540 and 595 nm was used to improve the sensitivity in signal detection. In addition, proteoglycan distribution was visualized via Alcian blue staining ($n = 2$). Deparaffinized sections were exposed to 3% acetic acid for 3 min, stained with Alcian blue for 45 min, and rinsed twice with acid-alcohol (pH = 1) for 1 min.[39]

Mineralization and calcified cartilage-related markers

Alkaline phosphatase (ALP) activity ($n = 5$) was measured using a colorimetric assay based on the hydrolysis of *p*-nitrophenyl phosphate (*p*NP-PO_4) to *p*-nitrophenol (pNP).[40] Briefly, the samples were lysed in 0.1% Triton™ X solution, exposed to a freeze–thaw cycle, and crushed with a mortar. A 25 μL aliquot was added to *p*NP-PO_4 solution (Sigma) and incubated for 10 min at 37°C. Absorbance was measured at 405 nm using a microplate reader (Tecan). In addition, calcium distribution ($n = 2$) was evaluated as an indicator of overall mineral distribution.[41] Briefly, deparaffinized histology sections were stained with alizarin red for 1 hour, rinsed with tap water, and differentiated in 0.01*N* HCl in 70% ethanol for 2 min. Media calcium concentration ($n = 5$) was quantified using the Arsenazo III dye (Pointe Scientific, Lincoln Park, MI), with absorbance measured at 620 nm with a microplate reader.[42]

The expression ($n = 3$) of collagen X, matrix metalloproteinase-13 (MMP-13), Indian Hedgehog (*Ihh)*, Runt-related transcription factor 2 (Runx 2), and parathyroid

TABLE I. Primer Sequences for Gene Expression.

Gene	Sense	Antisense	Amplicon Size (bp)
Col X	TGGATCCAAAGGCGATGTG	GCCCAGTAGGTCCATTAAGGC	82
Ihh	ATCTCGGTGATGAACCAGTG	CCTTCGTAATGCAGCGACT	97
MMP13	ACATCCCAAAACGCCAGACAA	GATGCAGCCGCCAGAAGAAT	109
PTHrP	ACCTCGGAGGTGTCCCCTAA	GCCCTCATCATCAGACCCAA	80
Runx2	AATCCTCCCCAAGTTGCCA	TTCTGTCTGTGCCTTCTGGGT	82
GAPDH	GCTGGTGCTGAGTATGTGGT	CAGAAGGTGCAGAGATGATGA	213

hormone-related protein (PTHrP) were measured at day 7 using reverse transcription followed by polymerase chain reaction (RT-PCR), with custom-designed primers (Table I). Briefly, total RNA was isolated via TRIzol (Invitrogen, Carlsbad, CA) extraction, then reverse-transcribed into cDNA using the SuperScript III First-Strand Synthesis System (Invitrogen). The cDNA product was amplified with recombinant Platinum Taq DNA polymerase (Invitrogen). Expression band intensities of relevant genes were analyzed semi-quantitatively and normalized to the housekeeping gene glyceraldehydes 3-phosphate dehydrogenase (GAPDH).

Statistical analyses

Results are presented in the form of mean ± standard deviation, with n equal to the number of samples analyzed per group. A two-way analysis of variance (ANOVA) was performed to determine the effects of ceramic type and culturing time on cell response (proliferation, matrix deposition, ALP activity, solution calcium concentration, gene expression), as well as scaffold parameters (weight, thickness, or water content). The Tukey-Kramer *post hoc* test was used for all pair-wise comparisons, and significance was attained at $p < 0.05$. All statistical analyses were performed using JMP 4.0.4 (SAS Institute, Cary, NC).

RESULTS

Ceramic characterization

Ceramic particle shape, calcium and phosphorus content, crystallinity, and chemistry are summarized in Figure 1. Electron microscopy revealed a shard-like morphology for CDA-1 and a globular shape for CDA-2 particles. Brightfield microscopy revealed that the CDA-1 particles were significantly larger than the CDA-2 particles (30.1 ± 10.5 μm and 11.9 ± 9.2 μm, respectively). Crystal planes (002, 211, 300, and 202) were identified in the XRD spectra of both ceramics, which are also found in the hydroxyapatite spectra (JCPDS 9–432, Fig. 1). Furthermore, the broad peaks in both spectra indicate that the ceramics are poorly crystalline. Analysis by FTIR confirmed phosphate presence via bending peaks corresponding to three vibrational modes (961, 1030–1080, 566–628 cm^{-1}), as well as hydroxyl (3568 cm^{-1}) and carbonate peaks (1415–1647 cm^{-1} 870 cm^{-1})[33,43,44] in both ceramics tested. In terms of molar Ca/P ratio, CDA-1 and CDA-2 were both calcium-deficient, with CDA-1 exhibiting a significantly lower Ca/P molar ratio than CDA-2, at 1.35 ± 0.01 and 1.41 ± 0.02, respectively. While there was no significant difference in weight fraction for combined calcium and phosphorus content, these two types of ceramics did differ in terms of calcium and phosphorus weight fractions ($p < 0.05$), with a higher calcium and lower phosphorus content measured for CDA-2 compared to CDA-1.

Composite scaffold characterization

Acellular control and ceramic-containing scaffolds were characterized in terms of scaffold size, water and ash weight, elemental composition, particle distribution and crystallinity (Fig. 2). Visually, the agarose-only scaffolds appeared transparent and topographically smooth under environmental scanning electron microscopy; whereas the ceramic-containing hydrogels were opaque, with uniformly distributed shard-like particles for the CDA-1 scaffolds and globular particles for the CDA-2 scaffolds (Fig. 2). No significant differences in scaffold height or diameter were detected between groups. Ceramic content, determined via thermogravimetric analysis, was found to be similar for the two ceramic scaffolds, accounting for 34.06 ± 5.5% of the CDA-1 scaffold dry weight and 35.8 ± 0.7% of the CDA-2 scaffold dry weight. Lower water content ($p < 0.05$) was measured for the ceramic-containing scaffolds compared to the ceramic-free control, although no significant difference was detected between the two ceramic-containing groups. No differences were detected in mechanical properties between the two ceramic-containing scaffold groups; however, the Young's modulus measured for the CDA-1 scaffolds was significantly lower ($p < 0.05$) than that of the ceramic-free control. Energy-dispersive X-ray analysis confirmed the presence of peaks for carbon, oxygen, sodium, phosphorus, and chloride in all scaffolds, which are related to the agarose and phosphate buffered solution used. Calcium, however, was only detected in the ceramic-containing hydrogel groups. X-ray diffraction analysis revealed that particles in the ceramic-containing scaffolds exhibited the same crystalline peaks (002, 211, 300, and 202) as the unincorporated ceramics (Fig. 2). Two background peaks, consistent with the peaks present for phosphate buffer saline, were also detected.

Cell growth and matrix deposition

Chondrocytes were viable in all scaffolds at day 14 (Fig. 3). Hematoxylin and eosin staining confirmed uniform cell distribution throughout the scaffolds. Between day 7 and 14, cell number increased for the ceramic-free control and the CDA-2 group, with the highest cell number detected in the CDA-2 group (Fig. 3).

Matrix was uniformly deposited throughout all scaffolds over time (Fig. 4). Glycosaminoglycan (GAG) content increased

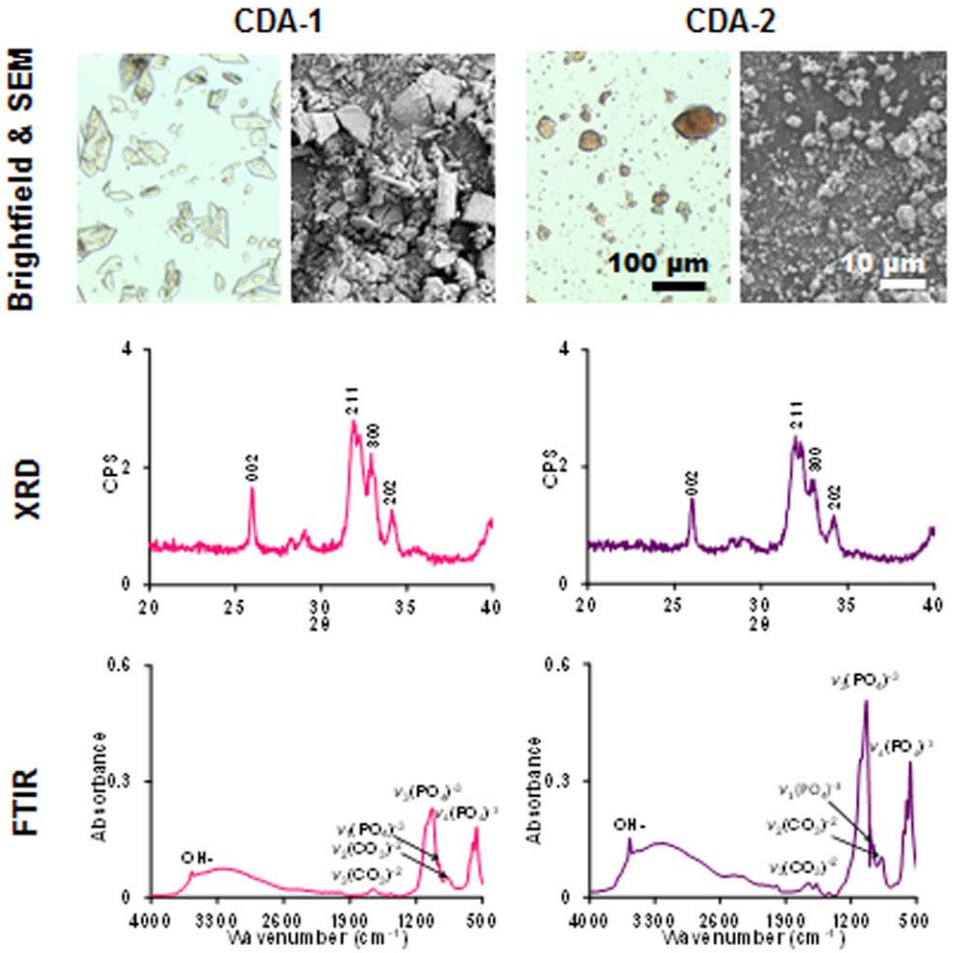

Parameter	CDA-1	CDA-2
Ca (wt%, n=6)	31.04 ± 0.22	31.58 ± 0.36*
P (wt%, n=6)	17.77 ± 0.11	17.35 ± 0.14*
Ca/P Molar Ratio (n=6)	1.35 ± 0.01	1.41 ± 0.02*

FIGURE 1. Ceramic characterization. Brightfield (20×, $n = 2$) and scanning electron microscopy (1000×, $n = 2$) reveal differences in particle shape between calcium phosphate powders. Characteristic phosphate bending curves as well as hydroxyl and carbonate peaks were identified with FTIR ($n = 2$). XRD ($n = 2$) shows that both powders are poorly crystalline. CDA-1 was found to have significantly lower calcium/phosphorus ratio than CDA-2 as determined via inductively coupled plasma analysis ($n = 6$, difference between CDA-1 and CDA-2 *$p < 0.05$).

significantly for the ceramic containing groups by day 7 and for all groups between day 7 and day 14. The highest GAG content was detected in the CDA-2 group at day 14 ($p < 0.05$). In terms of collagen deposition, a significant increase ($p < 0.05$) was measured for the ceramic-containing groups between day 1 and day 7, and for all groups between day 7 and day 14. Collagen content was significantly higher ($p < 0.05$) in ceramic-containing scaffolds than the control at day 7; however by day 14, no difference was found between groups. In addition, while no positive staining for collagen I was observed, collagen II was present in all scaffold groups examined (Fig. 4).

Chondrocyte mineralization and hypertrophy

In terms of ALP activity, the enzyme activity in the CDA-2 group decreased ($p < 0.05$) between day 1 and day 7, remaining at a basal level thereafter. Similarly for the CDA-1 and control groups, ALP activity also decreased over time. At day 14, positive alizarin red staining was observed in

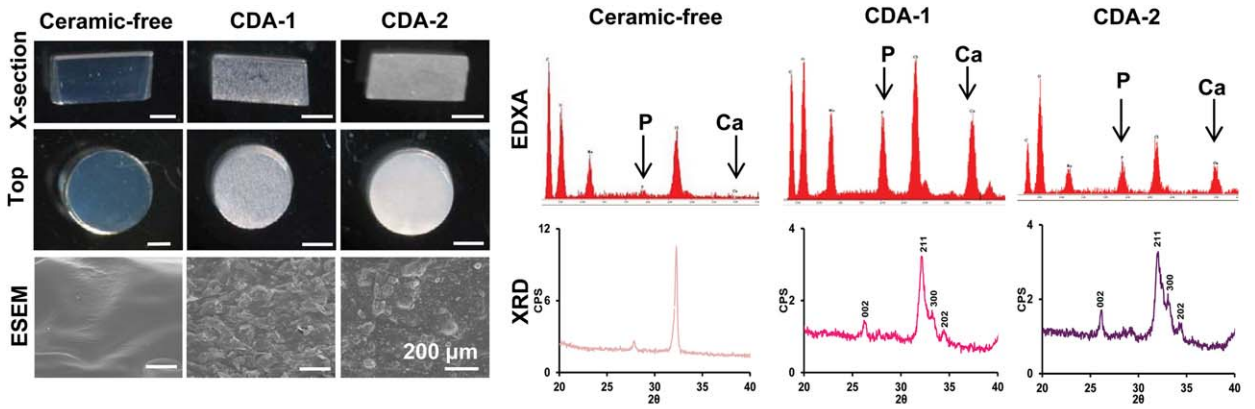

Parameter (n=3)	Ceramic-free	CDA-1	CDA-2
Height (mm)	2.2 ± 0.1	2.3 ± 0.1	2.3 ± 0.1
Diameter (mm)	4.8 ± 0.1	4.9 ± 0.1	4.9 ± 0.1
Ceramic content (% DW)	0 ± 0.1	34.06 ± 5.5	35.82 ± 0.7
Water content (%)	97.8 ± 0.2	95.7 ± 0.1*	96.2 ± 0.7*
Young's Modulus (kPa)	6.2 ± 0.7	4.1 ± 0.1*	4.9 ± 0.7
Dynamic Shear Modulus (kPa)	10.9 ± 1.1	7.6 ± 1.1	9.1 ± 2.5
Phase Shift Angle (degrees)	0.78 ± 0.8	1.2 ± 0.7	1.3 ± 0.7

FIGURE 2. As-fabricated acellular scaffold characterization. Scaffold cross-section and top-view images show uniform construct shape (stereoscope image, scale bar = 2 mm, $n = 3$) and size in terms of height and diameter ($n = 3$). ESEM reveals homogeneous particle distribution throughout the hydrogel. EDXA analysis confirms phosphorus and calcium content and XRD further confirms ceramic incorporation as the crystalline peaks present for both ceramics are also present in the composite scaffolds. The ceramic containing scaffolds have lower water content with respect to the ceramic-free control scaffolds. ($n = 3$, $^*p < 0.05$). Mechanical testing ($n = 3$) revealed similar mechanical properties for the ceramic-containing scaffolds, although a lower young's modulus was measured for CDA-1 scaffolds with respect to the ceramic free control.

CDA-1 and CDA-2 groups at day 14, with no detectable staining evident in the ceramic-free control.

Differences in hypertrophic markers were observed between groups at day 7. Downregulation of collagen X expression was measured for the CDA-2 group when compared to the ceramic-free control. The expression of Runx2 was also downregulated ($p < 0.05$) in the CDA-2 group, when compared to the CDA-1 group. In contrast, *Ihh* was upregulated ($p < 0.05$) for the CDA-1 group when compared to both the ceramic-free control and the CDA-2 containing group. Collagen X deposition was visualized via immunohistochemistry. It was detected in the ceramic groups on day 7 but was absent in the ceramic-free control (Fig. 5).

DISCUSSION

This study investigated the effect of ceramic composition on the ability of chondrocytes to form a calcified cartilage-like matrix in hydrogel-ceramic composite scaffolds. Specifically, composite scaffolds with distinct ceramic Ca/P ratios were formed, and it was observed that the scaffold with calcium/phosphorus molar

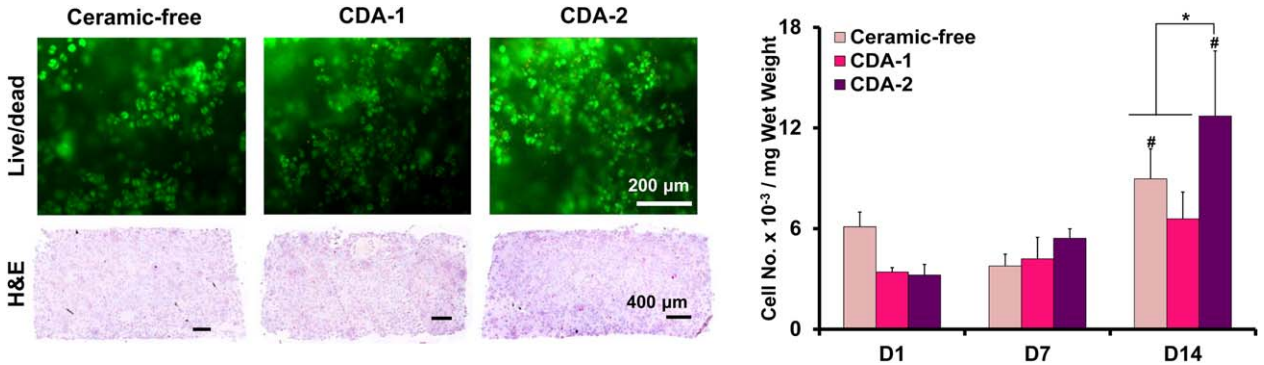

FIGURE 3. Cell viability, distribution, and number. Live/dead staining on day 14 detects viable cells in all groups (10×, bar = 200 μm, $n = 2$). Hematoxylin and eosin staining reveals uniform cell distribution throughout the scaffolds at day 14 (5×, bar = 400 μm, day 14, $n = 2$). Cell number increased over time with the highest cell number measured for the CDA-2 group at day 14 ($n = 5$, $^*p < 0.05$ for difference between groups, $\#p < 0.05$, for difference from corresponding group at previous time point).

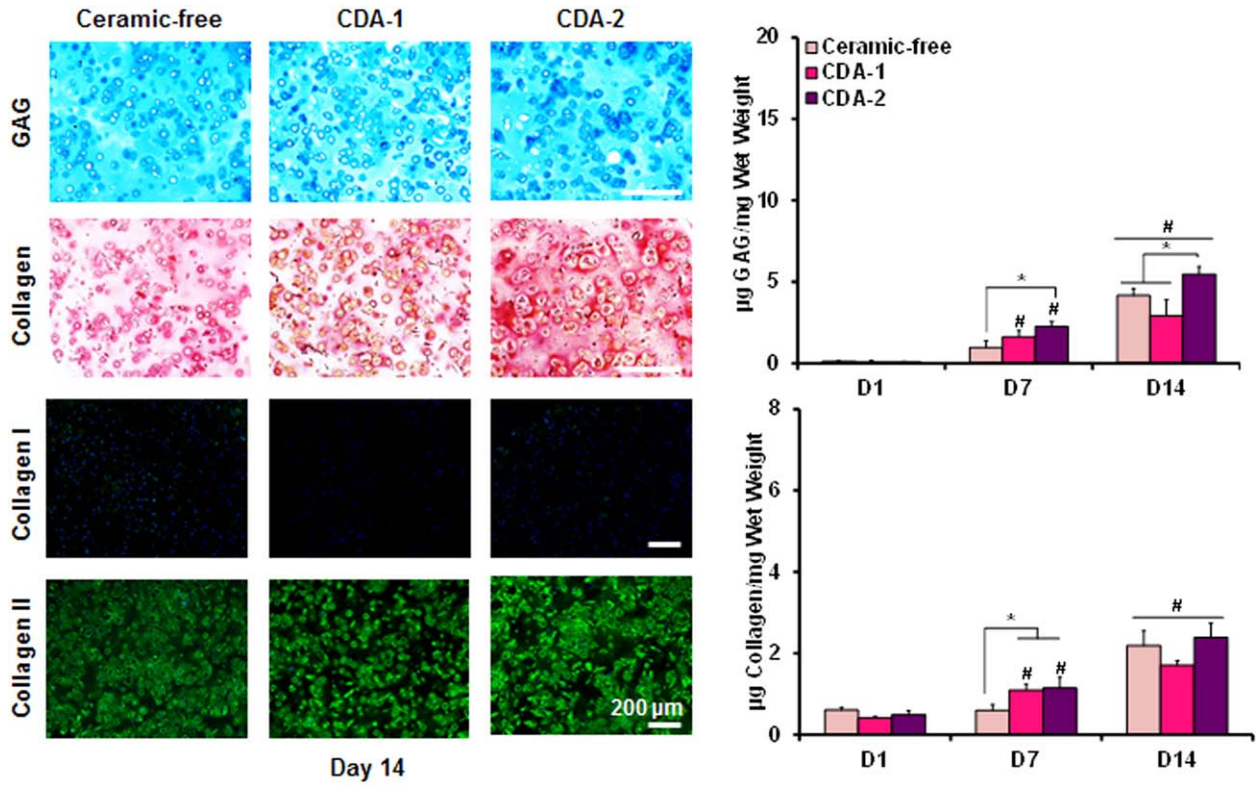

FIGURE 4. Matrix deposition. Significantly higher GAG and collagen deposition is detected on day 7 than on day 1 for both ceramic groups ($n = 5$,$^*p < 0.05$ for difference between groups, $\#p < 0.05$, for difference from corresponding group at previous time point). By day 14, histology reveals strongly positive matrix staining for all groups (alcian blue for GAG and picrosirius red for collagen, 10×, bar = 200 μm, day 14, $n = 2$). The CDA-2 group measured the highest GAG by day 14 ($n = 5$, $^*p < 0.05$). There was no difference between groups in terms of collagen deposition at day 14. All groups deposited a matrix rich in collagen type II and void of collagen type I (immunohistochemistry, 10×, bar = 200 μm, day 14, $n = 2$).

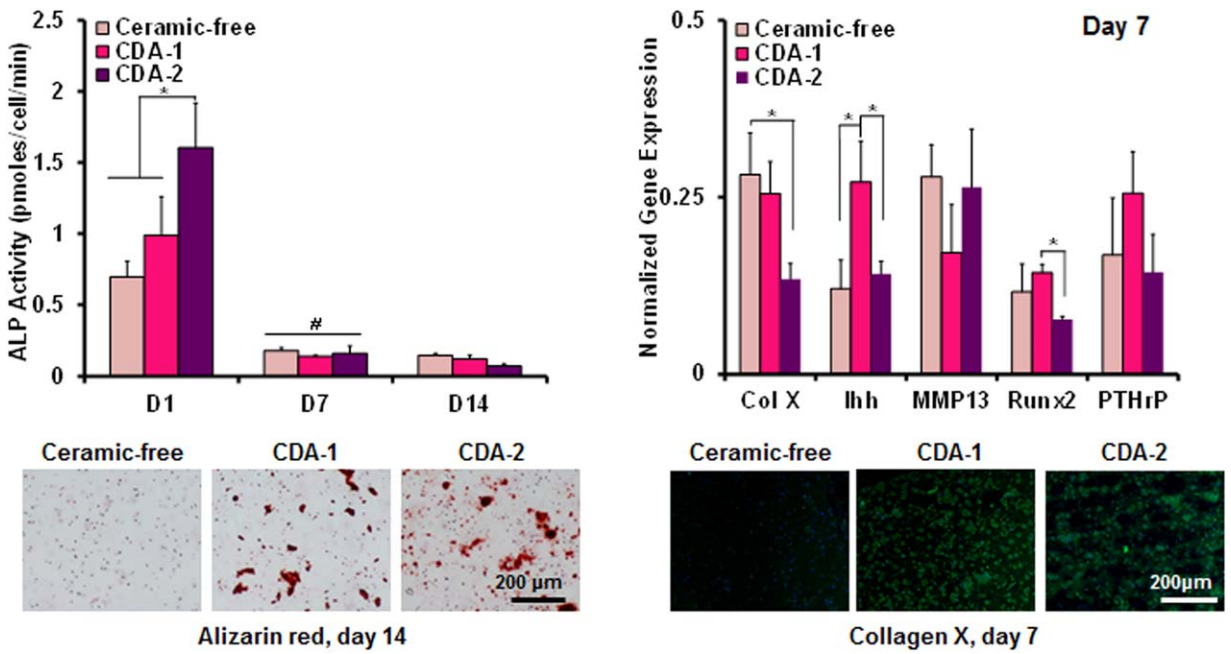

FIGURE 5. Mineralization. The highest ALP activity at day 1 was measured for the CDA-2 group ($n = 5$, $^*p < 0.05$). Similar ALP activity was measured for all groups at day 7 and day 14 with similar calcium staining on day 14 for ceramic groups (alizarin red, 10×, bar = 200 μm, day 14, $n = 2$). Collagen X and Runx 2 expression are downregulated on day 7 for the CDA-2 group and *Ihh* is upregulated of for the CDA-1 group (PCR, $n = 3$, $^*p < 0.05$). Collagen X immunohistochemistry staining is positive for collagen X in the ceramic groups on day 7 and negative for the control (immunohistochemistry, 20×, bar = 200 μm, day 14, $n = 2$).

ratio of 1.41 significantly promoted chondrocyte proliferation and matrix production, resulting in a dense matrix that was rich in both collagen II and proteoglycans. In contrast, ceramic particles with a Ca/P ratio of 1.35 had little effect on cell proliferation or matrix production. Collectively, these results illustrate that the cells are sensitive to changes in ceramic chemistry, and Ca/P ratio is an important parameter guiding cell growth and biosynthesis.

While the findings of this study confirm published results that calcium phosphates support chondrocyte proliferation and biosynthesis,[45,46] the mechanisms of this effect remain elusive. In this study, CDA-1 and CDA-2 differed significantly in Ca/P ratio, while exhibiting comparable crystallinity. To date, the response of chondrocytes to Ca/P ratio is unknown; however, published reports in bone-related studies have demonstrated that ceramic chemistry plays a central role in osteoblast adhesion, proliferation, and matrix deposition.[28–30] For example, Ergun et al. compared osteoblast response on eight calcium phosphate substrates and reported that increasing Ca/P ratio lead to increased osteoblast adhesion *in vitro*. In our study, initial seeding cell seeding was controlled as cells were encapsulated in agarose during scaffold fabrication; however, a higher Ca/P ratio of 1.41 led to increased chondrocyte proliferation and proteoglycan production during *in vitro* culture. Notably, in this study, the effect of crystal structure was controlled as the ceramics displayed similar structures. This insight helps to identify a key parameter to inform the design of composite systems for calcified cartilage formation.

In addition to enhanced matrix production, CDA-2 promoted early onset of alkaline phosphatase activity, which is likely related to the precipitation of calcium ions into the scaffolds, as indicated by the significant decrease in medium calcium concentration at day 1 for the ceramic-containing scaffolds (data not shown). A similarly early onset of alkaline phosphatase activity has been reported on day 1 for deep zone chondrocytes cultured in alginate hydrogel scaffolds,[25] a matrix rich in calcium crosslinks. The elevated bioavailability of calcium ions in both these systems may play a role in stimulating alkaline phosphatase production, as it has been reported that calcium concentration plays a role in regulating enzyme activity in chondrocytes.[47] In the current study, a similar decrease in media calcium was seen for both ceramic groups at early time points; however, elevated alkaline phosphatase activity was observed only for the CDA-2 group, indicating that multiple factors may be responsible for the observed elevation in enzyme activity, such as particle shape and roughness. In addition, differences in local calcium ion availability within the agarose gels proximate to the cells may have driven changes between the groups. Ion concentration in the micro environment within the scaffolds was not measured in this study and should be explored in future studies.

Following the early alkaline phosphatase activity enhancement, low activity was detected for all groups by day 7, with no difference evident between groups. Moreover, at day 7, culturing with CDA-2 resulted in downregulated collagen X expression, indicating that the deep zone chondrocytes did not become hypertrophic over time as was observed for those in the alginate scaffolds. This may be caused by a difference in calcium environments between the two systems as the alginate system provides high local calcium concentrations, or because of the inherent differences between the hydrogel networks which were used. In the current system, however, the pre-incorporation of a biomimetic calcium phosphate source likely reduces the need for cell-mediated mineralization over time.

In addition to differences in calcium–phosphorus ratio, differences in macroscopic particle shape between the two ceramics may have contributed to the observed difference in cell response. It has been observed that rod shaped β-TCP particles result in significantly more bone formation in an *in vivo* rabbit femur model after implantation for six months when compared to globular β-TCP particles.[48] Future studies should investigate particle roughness, which may also play a role in chondrocyte response as this parameter is known to effect stem cell proliferation on ceramic substrates,[49] and surface area which may effect ceramic solubility and will be evaluated in future studies. Moreover, the observed differences in cell response will be validated *in vivo* using relevant bone healing models.

CONCLUSIONS

The results of this study demonstrate that chondrocyte proliferation and matrix production is promoted by CDA-2, a bioactive calcium-deficient apatite with a Ca/P ratio of 1.41. Moreover, deep zone chondrocytes seeded in a composite agarose-CDA-2 system produce a matrix that is rich in GAG and collagen II in the absence of any media supplementation. This cell-mediated matrix elaboration combined with the pre-incorporated mineral results in a matrix that may be useful for calcified cartilage tissue engineering or endochondral ossification.

REFERENCES

1. Osteoarthritis and you: Patient information from the CDC. J Pain Palliat Care Pharmacother 2010; 24:430–438.
2. Brown TD, Johnston RC, Saltzman CL, Marsh JL, Buckwalter JA. Posttraumatic osteoarthritis: A first estimate of incidence, prevalence, and burden of disease. J Orthop Trauma 2006;20:739–744.
3. Hunziker EB. Biologic repair of articular cartilage. Defect models in experimental animals and matrix requirements. Clin Orthop Relat Res 1999;S135–S146.
4. Wei X, Gao J, Messner K. Maturation-dependent repair of untreated osteochondral defects in the rabbit knee joint. J Biomed Mater Res 1997;34:63–72.
5. O'Driscoll SW, Keeley FW, Salter RB. Durability of regenerated articular cartilage produced by free autogenous periosteal grafts in major full-thickness defects in joint surfaces under the influence of continuous passive motion. A follow-up report at one year. J Bone Joint Surg Am 1988; 70:595–606.
6. Hunziker EB. Articular cartilage repair: Basic science and clinical progress. A review of the current status and prospects. Osteoarthr Cartilage 2002;10:432–463.
7. Bedi A, Feeley BT, Williams RJ III. Management of articular cartilage defects of the knee. J Bone Joint Surg Am 2010;92:994–1009.
8. Schaefer D, Martin I, Shastri P, Padera RF, Langer R, Freed LE, Vunjak-Novakovic G. *In vitro* generation of osteochondral composites. Biomaterials 2000;21:2599–2606.
9. Gao J, Dennis JE, Solchaga LA, Awadallah AS, Goldberg VM, Caplan AI. Tissue-engineered fabrication of an osteochondral composite graft using rat bone marrow-derived mesenchymal stem cells. Tissue Eng 2001;7:363–371.
10. Sherwood JK, Riley SL, Palazzolo R, Brown SC, Monkhouse DC, Coates M, Griffith LG, Landeen LK, Ratcliffe A. A three-dimensional

osteochondral composite scaffold for articular cartilage repair. Biomaterials 2002;23:4739–4751.
11. Cao T, Ho KH, Teoh SH. Scaffold design and in vitro study of osteochondral coculture in a three-dimensional porous polycaprolactone scaffold fabricated by fused deposition modeling. Tissue Eng 2003;9: S103–S112.
12. Tuli R, Nandi S, Li WJ, Tuli S, Huang X, Manner PA, Laquerriere P, Noth U, Hall DJ, Tuan RS. Human mesenchymal progenitor cell-based tissue engineering of a single-unit osteochondral construct. Tissue Eng 2004;10:1169–1179.
13. Alhadlaq A, Mao JJ. Tissue-engineered osteochondral constructs in the shape of an articular condyle. J Bone Joint Surg Am 2005; 87:936–944.
14. Tanaka T, Komaki H, Chazono M, Fujii K, Tanaka T, Komaki H, Chazono M, Fujii K. Use of a biphasic graft constructed with chondrocytes overlying a beta-tricalcium phosphate block in the treatment of rabbit osteochondral defects. Tissue Eng 2005;11:331–339.
15. Grayson WL, Bhumiratana S, Grace Chao PH, Hung CT, Vunjak-Novakovic G. Spatial regulation of human mesenchymal stem cell differentiation in engineered osteochondral constructs: Effects of pre-differentiation, soluble factors and medium perfusion. Osteoarthr Cartilage 2010;18:714–723.
16. Harley BA, Lynn AK, Wissner-Gross Z, Bonfield W, Yannas IV, Gibson LJ. Design of a multiphase osteochondral scaffold III: Fabrication of layered scaffolds with continuous interfaces. J Biomed Mater Res A 2010; 92:1078–1093.
17. Jiang J, Tang A, Ateshian GA, Guo XE, Hung CT, Lu HH. Bioactive stratified polymer ceramic-hydrogel scaffold for integrative osteochondral repair. Ann Biomed Eng 2010;38:2183–2196.
18. Marquass B, Somerson JS, Hepp P, Aigner T, Schwan S, Bader A, Josten C, Zscharnack M, Schulz RM. A novel MSC-seeded triphasic construct for the repair of osteochondral defects. J Orthop Res 2010;28:1586–1599.
19. Hunziker EB, Driesang IM, Saager C. Structural barrier principle for growth factor-based articular cartilage repair. Clin Orthop Relat Res 2001;S182–S189.
20. Boskey AL. Mineral-matrix interactions in bone and cartilage. Clin Orthop Relat Res 1992;281:244–274.
21. Arsenault AL, Grynpas MD. Crystals in calcified epiphyseal cartilage and cortical bone of the rat. Calcif Tissue Int 1988;43:219–225
22. Redler I, Mow VC, Zimny ML, Mansell J. The ultrastructure and biomechanical significance of the tidemark of articular cartilage. Clin Orthop Relat Res 1975;112:357–62
23. Bullough PG, Jagannath A. The morphology of the calcification front in articular cartilage. Its significance in joint function. J Bone Joint Surg Br 1983;65:72–78.
24. Kandel RA, Hurtig M, Grynpas M. Characterization of the mineral in calcified articular cartilagenous tissue formed in vitro. Tissue Eng 1999;5:25–34.
25. Khanarian NT, Jiang J, Wan LQ, Mow VC, Lu HH. A hydrogel-mineral composite scaffold for osteochondral interface tissue engineering. Tissue Eng Part A 2012;18:533–545.
26. Khanarian NT, Haney NM, Burga RA, Lu HH. A functional agarose-hydroxyapatite scaffold for osteochondral interface regeneration. Biomaterials 2012;33:5427–5258.
27. Marchi J, Ribeiro C, Bressiani AHD, Marques MM. Cell Response of Calcium Phosphate Based Ceramics, a Bone Substitute Material. Materials Research-Ibero-American Journal of Materials 2013;16:703–712.
28. Yuan HP, Fernandes H, Habibovic P, de Boer J, Barradas AMC, de Ruiter A, Walsh WR, van Blitterswijk CA, De Bruijn JD. Osteoinductive ceramics as a synthetic alternative to autologous bone grafting. Proc Natl Acad Sci USA 2010;107:13614–13619.
29. Ergun C, Liu HN, Webster TJ, Olcay E, Yilmaz S, Sahin FC. Increased osteoblast adhesion on nanoparticulate calcium phosphates with higher Ca/P ratios. J Biomed Mater Res A 2008;85A:236–241.
30. Liu HN, Yazici H, Ergun C, Webster TJ, Bermek H. An in vitro evaluation of the Ca/P ratio for the cytocompatibility of nano-to-micron particulate calcium phosphates for bone regeneration. Acta Biomater 2008;4:1472–1479.
31. Allan KS, Pilliar RM, Wang J, Grynpas MD, Kandel RA. Formation of biphasic constructs containing cartilage with a calcified zone interface. Tissue Eng 2007;13:167–177.
32. Jiang J, Leong NL, Mung JC, Hidaka C, Lu HH. Interaction between zonal populations of articular chondrocytes suppresses chondrocyte mineralization and this process is mediated by PTHrP. Osteoarthr Cartilage 2008;16:70–82.
33. Yao F, LeGeros JP, LeGeros RZ. Simultaneous incorporation of carbonate and fluoride in synthetic apatites: Effect on crystallographic and physico-chemical properties. Acta Biomater 2009;5: 2169–2177.
34. Kim YJ, Sah RL, Doong JY, Grodzinsky AJ. Fluorometric assay of DNA in cartilage explants using Hoechst 33258. Anal Biochem 1988;174:168–176.
35. Reddy GK, Enwemeka CS. A simplified method for the analysis of hydroxyproline in biological tissues. Clin Biochem 1996;29:225–229.
36. Enobakhare BO, Bader DL, Lee DA. Quantification of sulfated glycosaminoglycans in chondrocyte/alginate cultures, by use of 1,9-dimethylmethylene blue. Anal Biochem 1996;243:189–191.
37. Farndale RW, Sayers CA, Barrett AJ. A direct spectrophotometric microassay for sulfated glycosaminoglycans in cartilage cultures. Connect Tissue Res 1982;9:247–248.
38. Seibel MJ, Macaulay W, Jelsma R, Saed-Nejad F, Ratcliffe A. Antigenic properties of keratan sulfate: Influence of antigen structure, monoclonal antibodies, and antibody valency. Arch Biochem Biophys 1992; 296:410–418.
39. Jiang J, Nicoll SB, Lu HH. Co-culture of osteoblasts and chondrocytes modulates cellular differentiation *in vitro*. Biochem Biophys Res Commun 2005;338:762–770.
40. Lu HH, Kofron MD, El Amin SF, Attawia MA, Laurencin CT. In vitro bone formation using muscle-derived cells: A new paradigm for bone tissue engineering using polymer-bone morphogenetic protein matrices. Biochem Biophys Res Commun 2003;305:882–889.
41. Wang IE, Shan J, Choi R, Oh S, Kepler CK, Chen FH, Lu HH. Role of osteoblast-fibroblast interactions in the formation of the ligament-to-bone interface. J Orthop Res 2007;25:1609–1620.
42. Lu HH, Tang A, Oh SC, Spalazzi JP, Dionisio K. Compositional effects on the formation of a calcium phosphate layer and the response of osteoblast-like cells on polymer-bioactive glass composites. Biomaterials 2005;26:6323–6334.
43. Gadaleta SJ, Paschalis EP, Betts F, Mendelsohn R, Boskey AL. Fourier transform infrared spectroscopy of the solution-mediated conversion of amorphous calcium phosphate to hydroxyapatite: New correlations between X-ray diffraction and infrared data. Calcif Tissue Int 1996;58:9–16.
44. Chou YF, Dunn JC, Wu BM. In vitro response of MC3T3-E1 preosteoblasts within three-dimensional apatite-coated PLGA scaffolds. J Biomed Mater Res B Appl Biomater 2005;75:81–90.
45. Remy M, Leclercq X, Naji A, Harmand MF, Vert M. Behavior of human cells in contact with a poly (d, l-lactic acid) porous matrix after calcification using phosphatidylserine. J Bioact Compat Polym 2012;27:375–387.
46. Muller FA, Muller L, Hofmann I, Greil P, Wenzel MM, Staudenmaier R. Cellulose-based scaffold materials for cartilage tissue engineering. Biomaterials 2006;27:3955–3963.
47. Wang D, Canaff L, Davidson D, Corluka A, Liu H, Hendy GN, Henderson JE. Alterations in the sensing and transport of phosphate and calcium by differentiating chondrocytes. J Biol Chem 2001;276:33995–34005.
48. Okuda T, Ioku K, Yonezawa I, Minagi H, Kawachi G, Gonda Y, Murayama H, Shibata Y, Minami S, Kamihira S, Kurosawa H, Ikeda T. The effect of the microstructure of beta-tricalcium phosphate on the metabolism of subsequently formed bone tissue. Biomaterials 2007;28:2612–2621.
49. Deligianni DD, Katsala ND, Koutsoukos PG, Missirlis YF. Effect of surface roughness of hydroxyapatite on human bone marrow cell adhesion, proliferation, differentiation and detachment strength. Biomaterials 2000;22:87–96.